

**Interfacial regulation of dendrite-free zinc anodes through  
dynamic hydrophobic molecular membrane**

Xin Hao, Jiugang Hu\*, Zongju Zhang, Yuqing Luo, Hongshuai Hou,  
Guoqiang Zou, Xiaobo Ji

College of Chemistry and Chemical Engineering, Central South  
University, Changsha, 410083, China.

E-mail: [hujiugang@csu.edu.cn](mailto:hujiugang@csu.edu.cn)

## **Experimental section**

### **Materials**

Potassium hydroxide (KOH) and zinc oxide (ZnO) were analytical grade. The hydrophobic tetradecyl (trihexyl) phosphonium chloride) (denoted as IL101, molecular weight=519.32 g/mol) was purchased from J&K scientific Ltd (China) without further purification. Ultra-pure water (Millipore, 18.2MΩ/cm) was used throughout the experiment process. Zinc plate (99.9%) and commercial MnO<sub>2</sub>-based air electrode were purchased from Changsha Sprin New Energy Technology Ltd.

### **Modification of hydrophobic molecular membrane on electrific zinc electrode**

Briefly, a saturated-IL101 electrolyte was prepared by dissolving hydrophobic IL101 molecules in alkaline solution containing 6 mol/L KOH and 0.1 mol/L zinc ions (electrolyte A), where ZnO was previously dissolved into 6 mol/L KOH. After stirring vigorously overnight, excess IL101 was removed by centrifuge due to its hydrophobicity. For comparison, a IL101-free alkaline electrolyte containing 0.1 mol/L zinc ions and 6 mol/L KOH (electrolyte B) and a zinc-free alkaline electrolyte containing saturated-IL101 and 6 mol/L KOH (electrolyte C) was prepared, respectively. The DHM-modification of electrode was carried out in the prepared electrolyte (electrolyte C) with a two-electrode system, where a zinc plate was used as the working electrode, and a zinc sheet was used as the reference electrode and the counter electrode. The modification voltage is set to -0.5V through CHI660e electrochemical workstation and the modification time is 60s. After modification, the modified electrode was washed slightly with ultra-pure water. For comparison, a constant voltage of 0.5 V was applied on DHM-modified electrode to examine the IL101 state on the electrode surface. The chemical oxygen demand of the electrolyte

was measured to evaluate the content of IL101 in saturated-IL101 electrolyte using dichromate oxidation method. Through the catalysis role of  $\text{Ag}_2\text{SO}_4$ , the IL101 molecules were completely oxidized with  $\text{K}_2\text{Cr}_2\text{O}_4$  in a concentrated  $\text{H}_2\text{SO}_4$  medium. Based on the redox reaction of IL101, its content in the electrolyte can be calculated from the COD value (Figure S1).

### **Electrochemical experiments**

Electrochemical analysis was performed in a classic three-electrode system on CHI660e workstation with a glassy carbon electrode as the working electrode,  $\text{Hg}/\text{HgO}$  as the reference electrode, and a platinum metal plate as the counter electrode. Before test, the glassy carbon electrode was polished on a buckskin polishing cloth with  $0.05\ \mu\text{m}$  alumina powder until having a mirror surface, and then rinsed with deionized water three times and then dried naturally. Cyclic voltammetry curves were determined in both electrolyte A and electrolyte B between  $-1.15\ \text{V}$  and  $-1.75\ \text{V}$  at a sweeping rate of  $20\ \text{mV s}^{-1}$ . The current–time curves were determined during plating at  $-1.6\ \text{V}$ . A glassy carbon electrode (GCE), fresh zinc plate, and copper plate was used as the working electrode to evaluate the role of DHM on zinc deposits in both electrolyte A and electrolyte B. The volume of electrolyte is 20 mL. The corresponding electrode in different electrolytes was denoted as DHM-modified electrode and pristine electrode, respectively. Zinc deposits on copper plate were obtained in electrolyte A and electrolyte B at 0.5h, 1h, and 2h with a current density of  $10\ \text{mA}/\text{cm}^2$ , respectively.

### **In-situ X-ray imaging experiments**

The synchrotron in-situ imaging of zinc plating process was recorded at X-ray

Imaging and Biomedical Application Beamline (BL13W1) of Shanghai synchrotron Radiation Facility (SSRF). A homemade transparent polyethylene cell with length of 5cm, width of 1cm and height of 4 cm (as shown in Figure S5). The volume of the added electrolyte is 15 mL. A glassy carbon electrode (GCE), Ag/AgCl, and a platinum metal plate was used as the working electrode, reference electrode, and counter electrode. A constant voltage of -1.7 V was applied for the zinc plating process with an electrochemical workstation. During zinc plating/stripping process, the synchrotron radiation X-ray light is parallel to the electrode surface to collect the statistical information of zinc deposits. Therefore, after adding the electrolyte A or electrolyte B, the cross-section images of electrode/electrolyte interface can be clearly observed because of their density difference. Especially, when zinc was plated on the glassy carbon electrode, the high-density metallic zinc deposits can be in-situ captured due to the apparent difference of phase contrast among zinc, GCE, and aqueous electrolyte. The synchrotron beam was monochromatized to 30 keV. The X-ray images were collected at a temporal resolution of 1s and a spatial resolution of 0.665  $\mu\text{m}$ . The in-situ imaging view of 2048 pixels. The obtained raw images were processed with image pro plus 7 software.

### **Battery fabrication and electrochemical measurements**

The tests of Zn//Zn symmetry batteries and zinc-air batteries were performed in a self-made mold, where the cathode and anode were sandwiched between three polymethyl methacrylate components. The middle component of mold has a circular hole with an area of 3.14  $\text{cm}^2$  and two zinc sheets were severally assembled at two sides of middle component. The distance between the two electrodes is 0.8 cm. After adding the electrolyte A or B, the galvanostatic cycling of Zn//Zn symmetric batteries were

performed on LAND CT2001A at 25°C, the current density of 1.0 mA/cm<sup>2</sup>, and the plating/stripping time of 20 min. Before the experiment, the fresh zinc plate was polished with 6000 mesh sandpaper until the surface is bright, then washed with deionized water and acetone, and dried in air. Coulombic efficiency (CE) measurements were evaluated using reported method<sup>1,2</sup>.

A rechargeable zinc-air cell was constructed for the battery test (Fig. S15), where the polished zinc foil and the commercial MnO<sub>2</sub>-based air electrode were employed as the anode and cathode, respectively. Commercial air electrode was fabricated by  $\alpha$ -MnO<sub>2</sub> nanoparticles (<70 nm particle size, 99.9%) as bifunctional catalyst. The catalyst ink consists of 65 wt% acetylene black, 20 wt%  $\alpha$ -MnO<sub>2</sub>, and 15 wt% PTFE (aqueous solution). The loading catalyst on nickel mesh (0.2 mm thickness, 1.25×2.5 mm rhombic pore) was 1.2 mg cm<sup>-2</sup>. The electrolyte used in the zinc-air battery was 6 mol/L KOH and 0.1 mol/L ZnO. The galvanostatic charge and discharge (GDC) curves were collect at 10 mA/cm<sup>2</sup> and 30 min/cycle.

### **Characterization of deposits**

The surface morphology of zinc deposits was characterized by scanning electron microscopy (SEM; JSM-6360LV, JEOL, Japan). Because IL101 molecule has phosphorus-containing functional group, the element mapping of phosphorus on DHM-modified zinc was also determined with the energy dispersive X-ray detector of SEM. X-ray diffraction (XRD; Shimadzu XRD-7000S, Japan) was used to identify the crystal structure of zinc deposits. The contact angle values of the prepared electrolyte B on fresh zinc sheets or DHM-modified zinc were measured on a Contact Angle Geniometer (SDC-100, China) at 25 °C. The reported value is the average of the three measurements at different locations for each sample.

Table S1. The content of saturated hydrophobic IL101 in electrolyte

Electrolyte	COD (mg/L)	Content (mg/L)	Concentration (mmol/L)
IL101	125	41.0	0.08

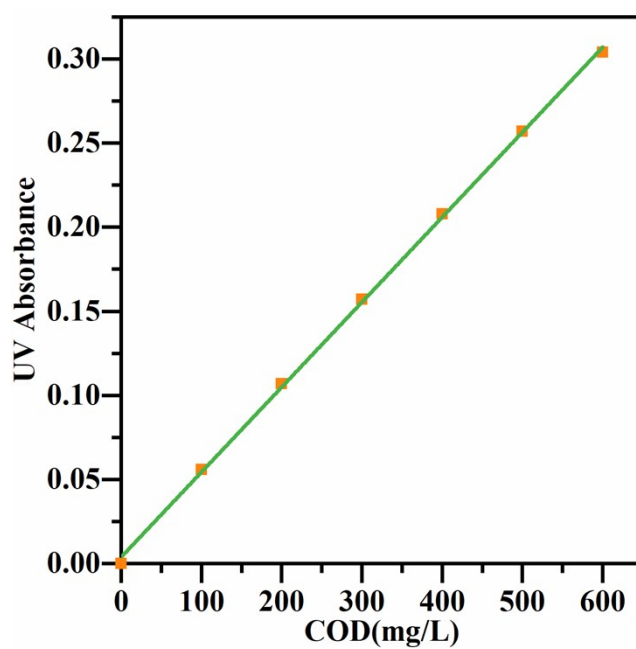
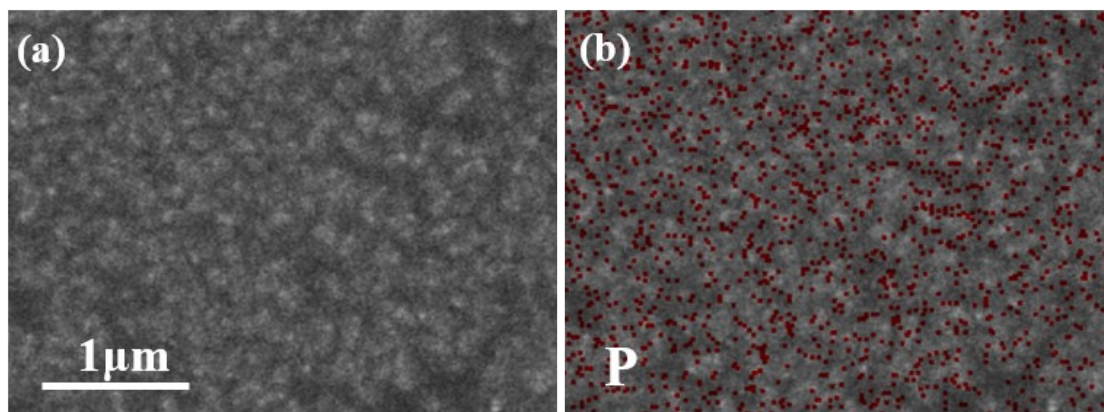
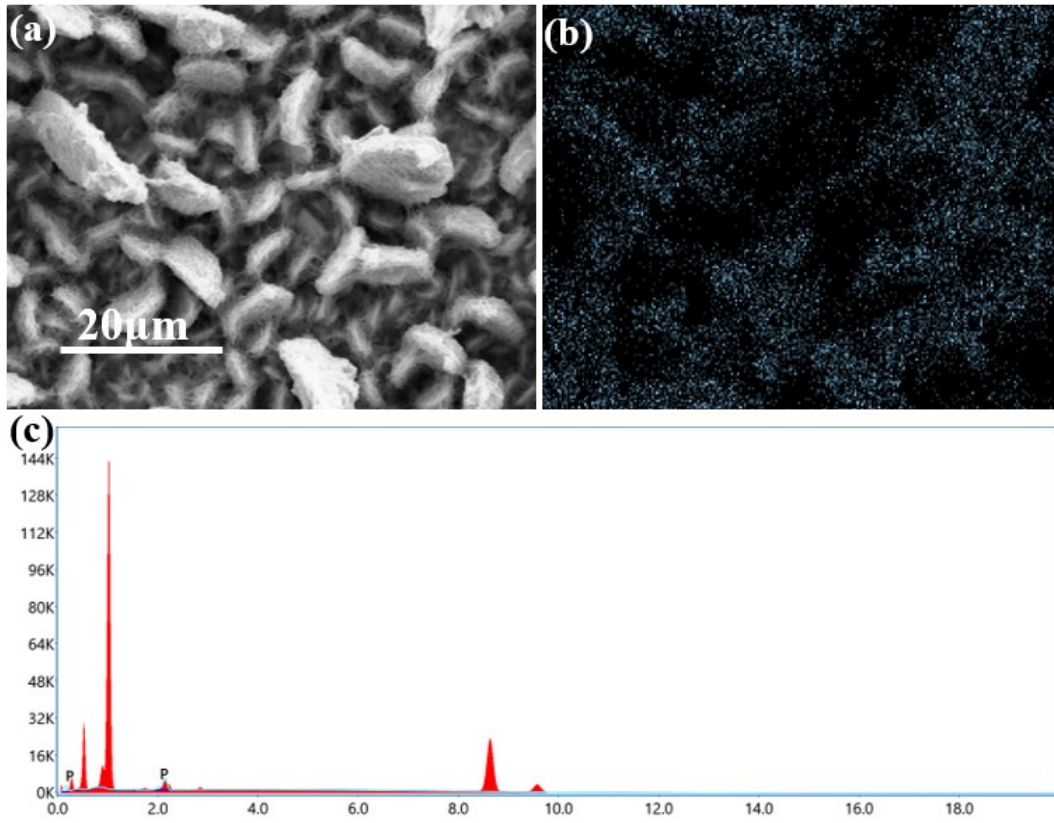


Figure S1. COD calibration curve of standard solutions.



**Figure S2.** (a) SEM and (b) element mapping image of phosphorus on DHM-modified zinc anode.



**Figure S3.** (a) SEM, (b) element mapping image of phosphorus, and (c) EDS energy spectrum of zinc deposits obtained at 5 mAh/cm<sup>2</sup>.



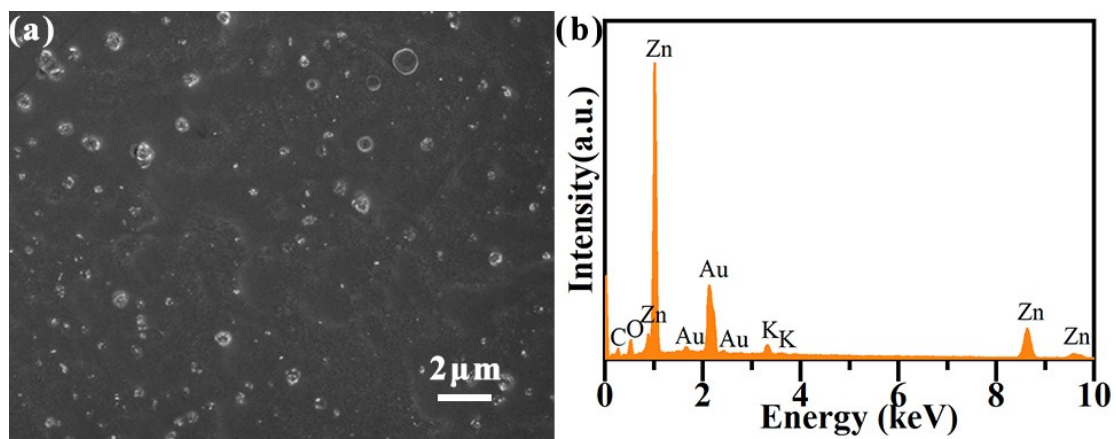


**Figure S4.** (a) SEM and (b) EDS energy spectrum of DHM-modified electrode after applied a positive constant voltage of 0.5 V.

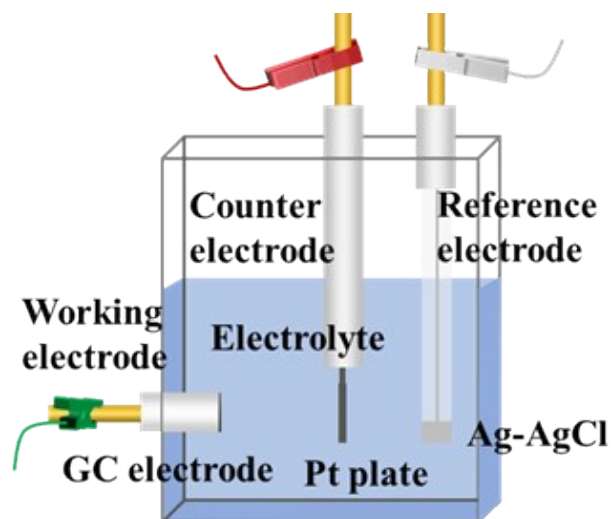


**Figure S5.** Schematic illustration of self-made test device for in-situ X-ray imaging.

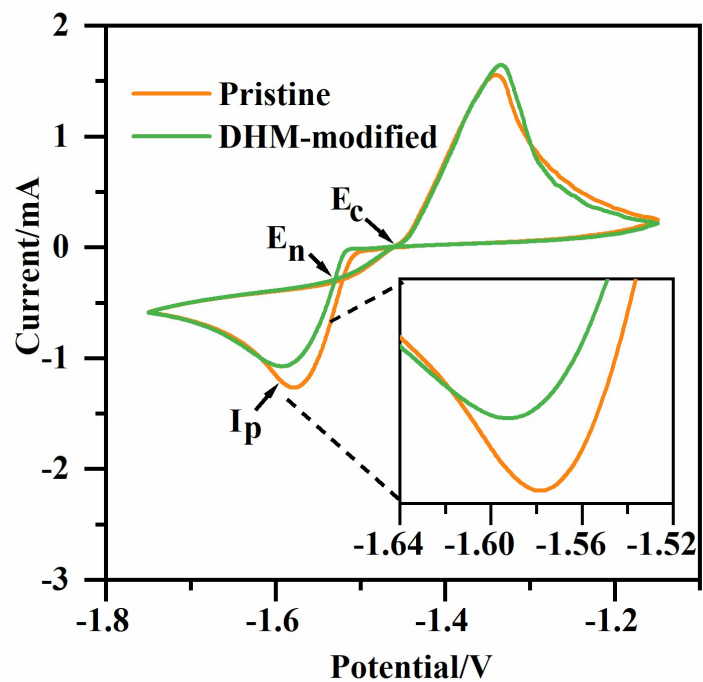


**Figure S6.** CV curves of zinc species at scanning rate of 20 mV/s between -1.75 V and -1.15 V (vs Hg/HgO).

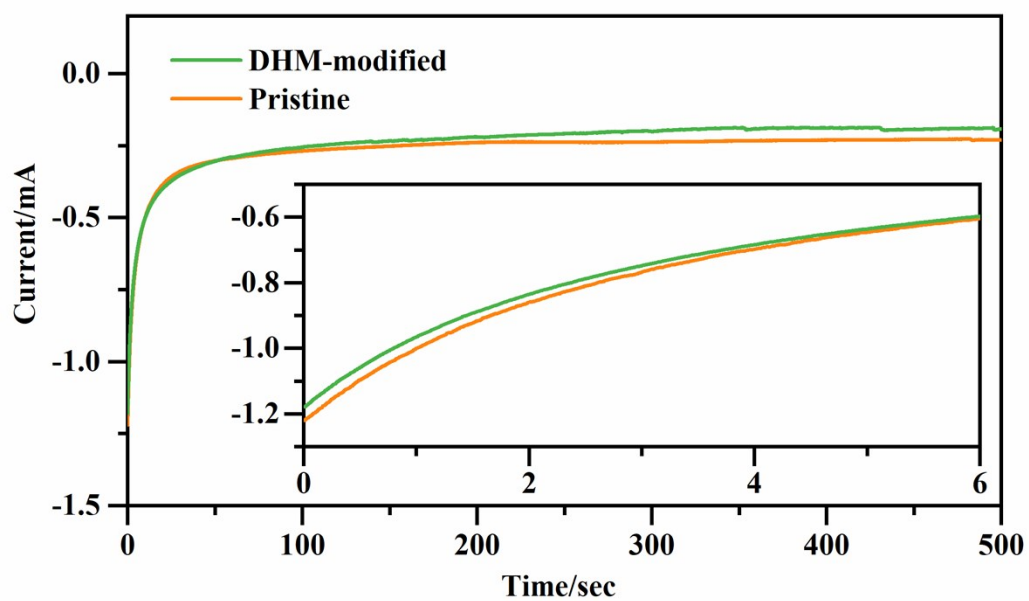


**Figure S7.** Current-time curves of zinc plating process (Potential: -1.6 V vs Hg/HgO; Time: 500s).

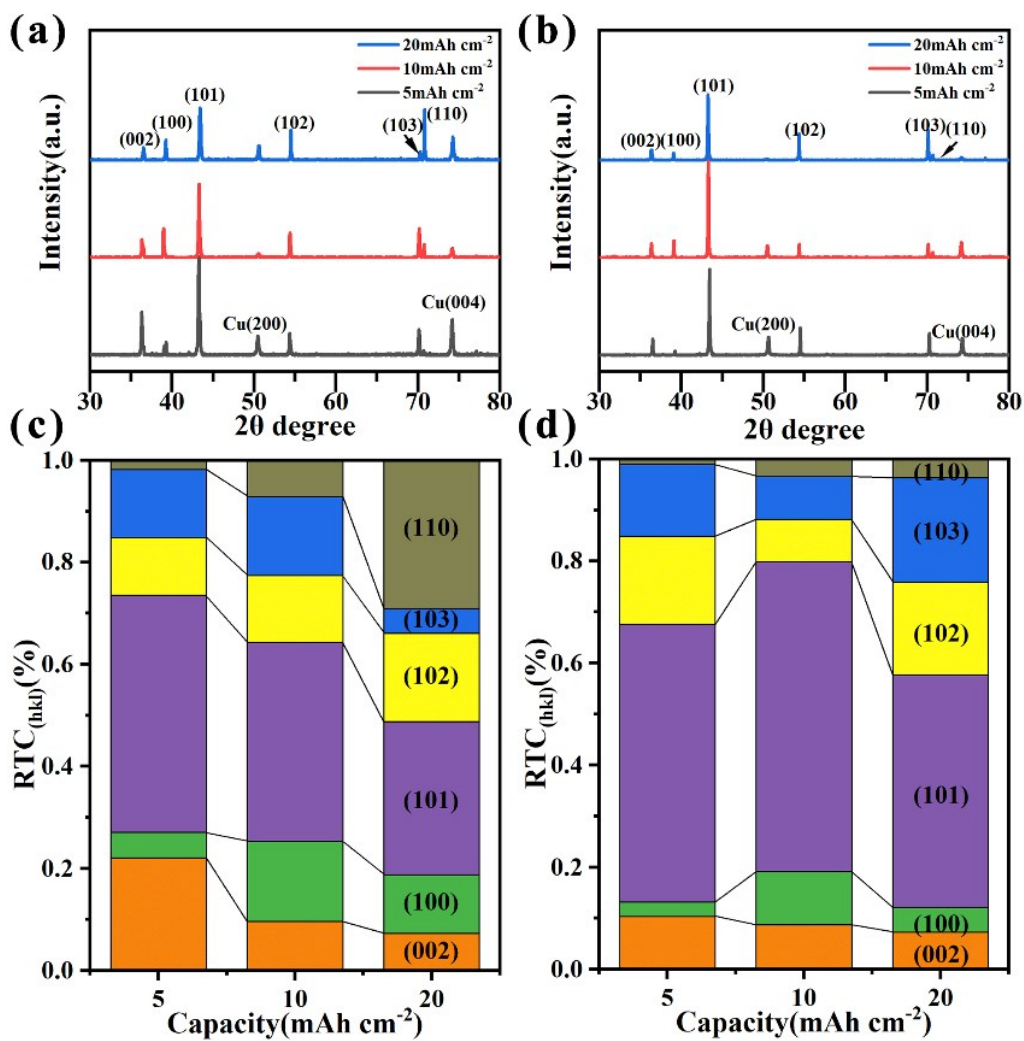


**Figure S8.** XRD patterns and relative texture coefficient of zinc deposits on copper substrate with different charge capacities. (a, c) pristine electrode, (b, d) DHM-modified electrode.

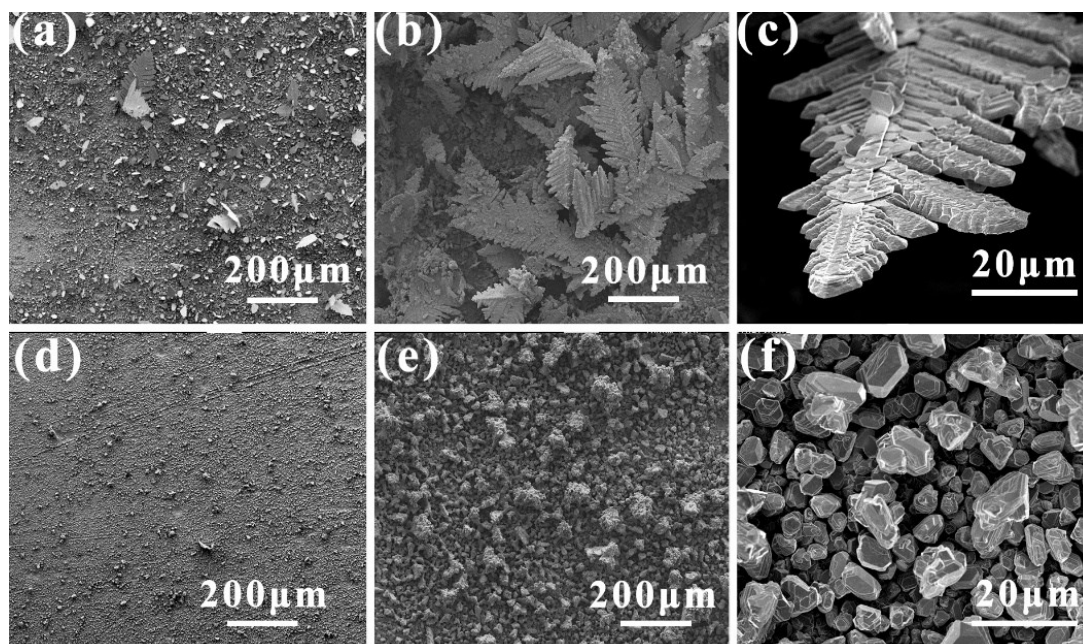


**Figure S9.** SEM images of zinc deposits on copper substrate with different charge capacities (5, 10, 20 mAh/cm<sup>2</sup>, respectively). (a-c) pristine electrode, (d-f) DHM-modified electrode.

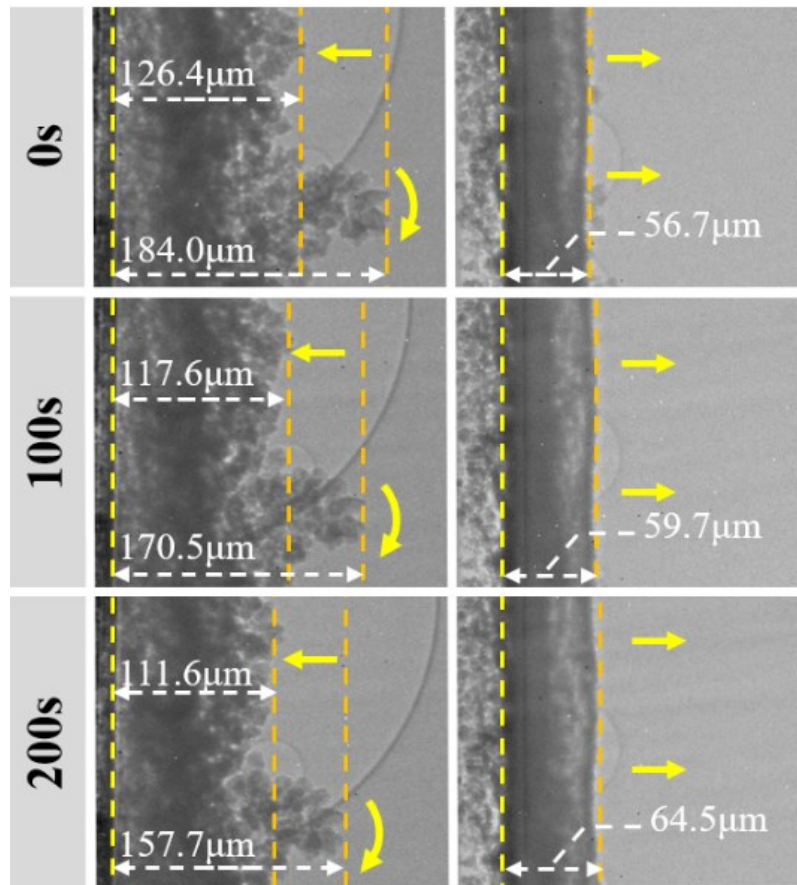


**Figure S10.** In-situ X-ray imaging images of self-discharge process of zinc deposits. (left) pristine electrode, (right) DHM-modified electrode.

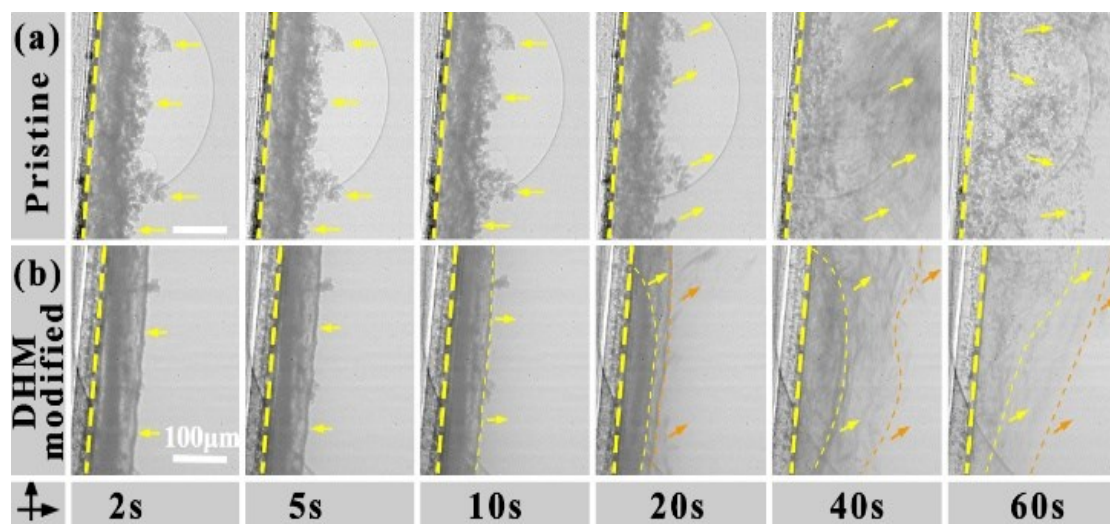


**Figure S11.** In-situ X-ray imaging images of zinc stripping process. (a) pristine electrode, (b) DHM-modified electrode. (-1.4 V, yellow arrows represent the evolution direction of zinc deposits)



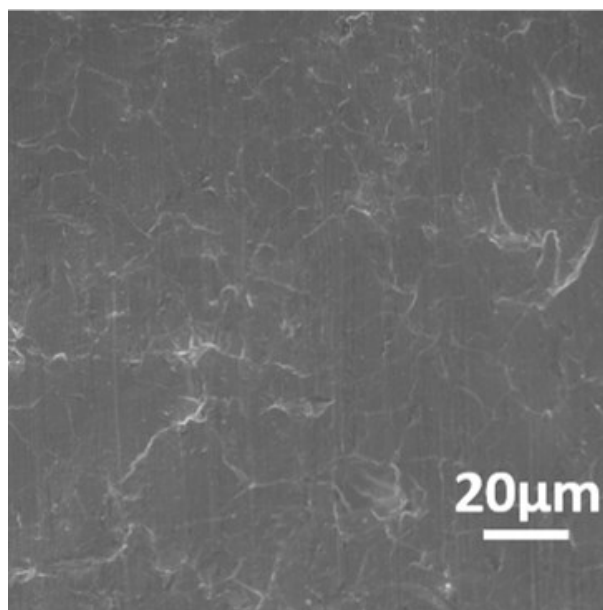


**Figure S12.** SEM image of original Zn plate.

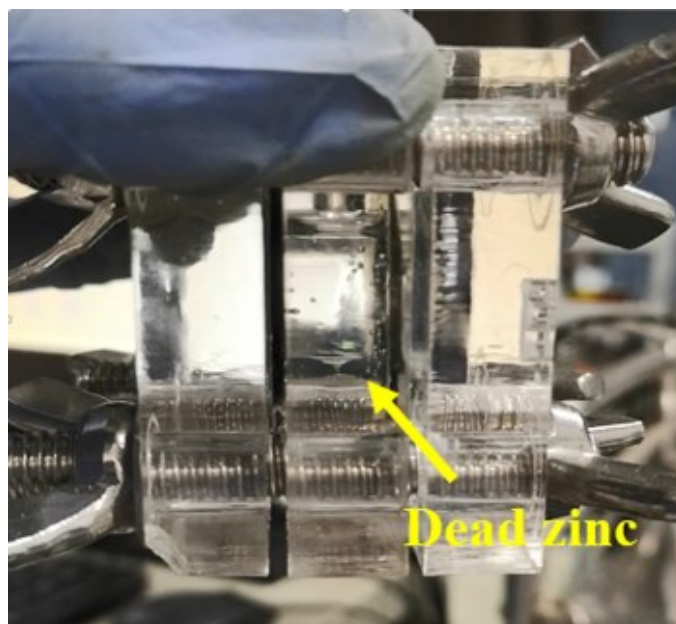


**Figure S13.** Optical image of the formed “dead zinc” in Zn//Zn symmetric cell.

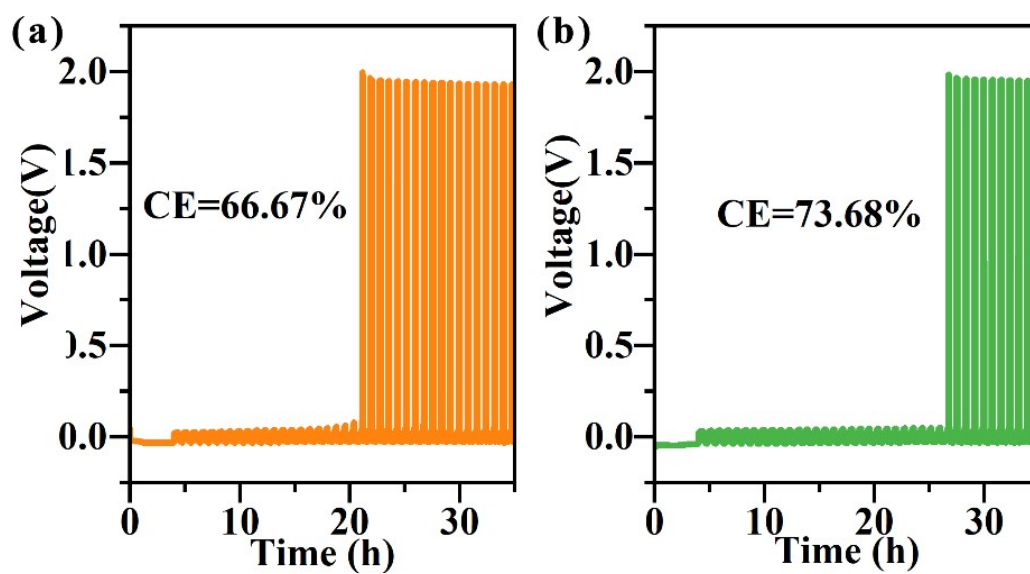


**Figure S14.** Average CE measurements of Zn plating/stripping process in asymmetric Zn//stainless steel cells.



**Figure S15.** Optical image of the mold for zinc-air battery.

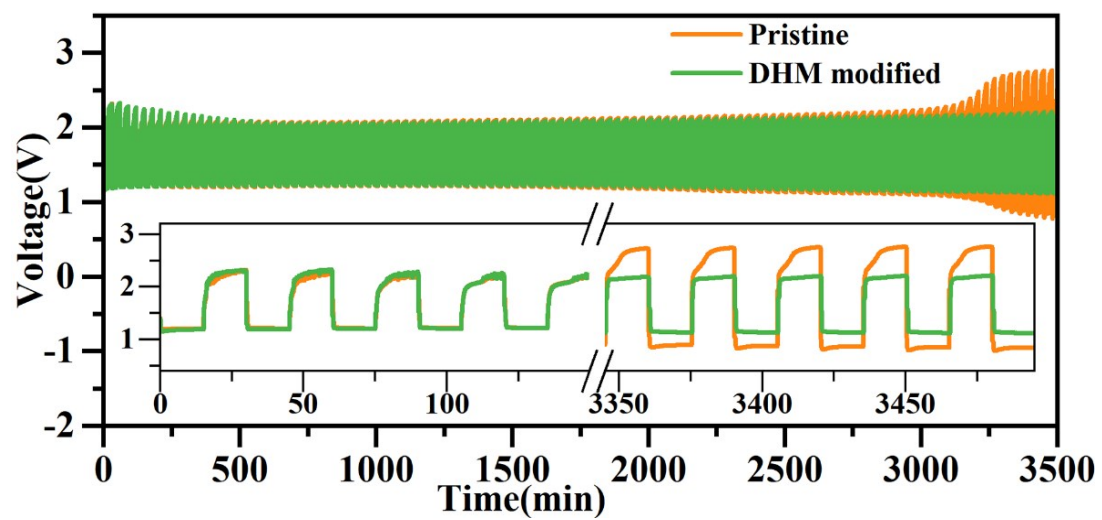


**Figure S16.** Discharge-charge cycles of zinc-air batteries at 10 mA/cm<sup>2</sup> and 30min/cycle

**References:**

1. C. Zhang, J. Holoubek, X. Wu, A. Daniyar, L. Zhu, C. Chen, D. P. Leonard, I. A. Rodriguez-Perez, J. X. Jiang, C. Fang and X. Ji, *Chemical communications*, 2018, **54**, 14097-14099.
2. B. D. Adams, J. Zheng, X. Ren, W. Xu and J.-G. Zhang, *Adv Energy Mater*, 2018, **8**, 1702097.